# DEVELOPMENT OF SECONDARY FLOW IN A CURVED RECTANGULAR DUCT

Amer Nordin Darus[*], Yap Yip Fatt
Department of Thermo-Fluids,
Faculty of Mechanical Engineering,
Universiti Teknologi Malaysia,
Skudai, Johor

## ABSTRACT

*Development of secondary flow in curved rectangular regular section duct using an improved finite difference scheme for solving parabolized Navier-Stokes equations is presented. This scheme has its origin in the work of Briley, which is based on ADI method to march the solution in the streamwise direction. With some modifications, it is shown in the present work that the stability of this scheme is greatly enhanced. Its applicability is considerably increased. To demonstrate the strength of the improved scheme, it is used to predict the flows in both mildly and strongly curved ducts for moderate to high Dean number. Predictions obtained with the improved scheme show good agreement with the available experimental and computational data.*

**Keywords**: *Secondary flow, curved rectangular duct, parabolised Navier-Stokes*

## 1.0 INTRODUCTION

The use of parabolized Navier-Stokes (PNS) equations to model internal flow problems has been gaining momentum. The main advantage of using PNS equations to simulate incompressible viscous flows is the suppression of elliptical behavior in the streamwise direction of the flow wherein the governing equations become parabolic in this direction. Thus, these equations are solvable by space-marching techniques, saving considerable storage and computational time.

The potential of PNS equations in predicting laminar flow in a curved circular pipe was tapped by Patankar *et al.* [1] using the scheme of Patankar and Spalding [2]. Their predictions show a very satisfactory agreement with the available experimental data of Mori and Nakayama [3] and Austin [4] and the theoretical solution of Akiyama and Cheng [5]. Thereafter, a number of investigators has followed the works of Patankar *et al.* [1] and even extended the use of PNS equations to developing flow in curved rectangular ducts.

Initial investigation on developing flow in a curved rectangular duct is attributed to Ghia and Sokhey [6]. By adopting Briley's [7] scheme, they obtained the solutions in ducts of $0.0100 \leq H_D/R_o \leq 0.2857$ ($H_D$ and $R_o$ are the hydraulic

---

[*] Corresponding author: E-mail: amer@fkm.utm.my

diameter and the mean radius of curvature of the duct respectively) for $51 \leq De \leq 350$ where the Dean number is defined as

$$De = Re \left( \frac{D_H}{R_o} \right)^{\frac{1}{2}}$$ (1a)

and

$$Re = \frac{\rho U_o D_H}{\mu}$$ (1b)

On the other hand, Govindan and Lakshminarayana [8] computed the developing flow in a curved duct of $H_D/R_o=0.0690$ for De=54 using a newly developed space-marching scheme. However, Humphrey *et al.* [9] is of the opinion that PNS equations are good approximation only for curved ducts with small curvature ratio, $H_D/R_o$. For strongly curved ducts, they advocate the use of partially PNS equations suggested by Pratap and Spalding [10]. With this approximation, Humphrey *et al.* [9] computed the developing flow in a curved square duct of $H_D/R_o=0.4348$ for De=520. It was later that Pouagare and Lakshminarayana [11] demonstrated the applicability of PNS equations in predicting developing flow in strongly curved ducts. Their solution for the case of $H_D/R_o=0.4348$ for De=520, as computed by Humphrey *et al.* [9], is in good agreement with the experimental data of Taylor *et al.* [12].

In the present study, the work of Ghia and Sokhey [6] on developing flow in a curved rectangular duct has been reproduced first. It is found that the scheme of Briley [7] is liable to numerical instability and at times even leads to divergent results when computations were made for either strongly curved ducts ($H_D/R_o > 0.2857$) or for the case of $De \geq 300$. Furthermore, it was discovered in the work of Yap [13], in which the scheme of Briley was used to simulate flows in a curved converging rectangular duct that numerical instability occurred even for duct with the slightest contraction. Thus, it is the intention of the present study to improve the stability of Briley's scheme through some modifications, paving the way for solving the PNS equations for flows in a curved converging rectangular duct. In order to demonstrate the potential and applicability of the modified scheme of Briley, the present study has extended the work of Ghia and Sokhey to the case of strongly curved ducts and of $De > 350$, cases where the original scheme of Briley is found insufficient. It will be shown that the present scheme is capable to produce results that are in good agreement to that of Rosenfeld *et al.* [14], Arnal *et al.* [15], Zang *et al.* [16] and Tamamidis *et al.* [17], some recent numerical solutions for fully elliptic Navier-Stokes equations.

## 2.0 MATHEMATICAL FORMULATION

### 2.1 Governing Equations
The geometry of a curved rectangular duct as depicted in Figure 1 can be conveniently represented in cylindrical coordinate (R, θ, Z). PNS equations are derivable from the Navier-Stokes equations by omitting the diffusive terms in the

streamwise direction together with the decoupling of the pressure term into an average pressure $(P_\theta(\theta))$ and a transverse pressure distribution $(P_{rz}(R,Z;\theta))$ as documented in Tannehill *et al.* [18]. It should be noted that $P_{rz}$ is a mild function of $\theta$ such that $\partial P_{rz}/\partial\theta$ is negligible. Thus, the static pressure, P, is the sum of $P_\theta$ and $P_{rz}$.

$$P = P_\theta + P_{rz} \tag{2}$$

Since $\theta$-direction is the streamwise direction, the governing PNS equations should read: R-momentum:

$$U_r \frac{\partial U_r}{\partial R} + \frac{U_\theta}{R}\frac{\partial U_r}{\partial\theta} + U_z \frac{\partial U_r}{\partial Z} - \frac{U_\theta^2}{R^2}$$
$$= -\frac{1}{\rho}\frac{\partial P_{rz}}{\partial R} + \frac{\mu}{\rho}\left[\frac{\partial^2 U_r}{\partial R^2} + \frac{1}{R}\frac{\partial U_r}{\partial R} + \frac{\partial^2 U_r}{\partial Z^2} - \frac{U_r}{R^2} - \frac{2}{R^2}\frac{\partial U_\theta}{\partial\theta}\right] \tag{3a}$$

$\theta$-momentum:

$$U_r \frac{\partial U_\theta}{\partial R} + \frac{U_\theta}{R}\frac{\partial U_\theta}{\partial\theta} + U_z \frac{\partial U_\theta}{\partial Z} - \frac{U_r U_\theta}{R^2}$$
$$= -\frac{1}{\rho}\frac{\partial P_\theta}{\partial\theta} + \frac{\mu}{\rho}\left[\frac{\partial^2 U_\theta}{\partial R^2} + \frac{1}{R}\frac{\partial U_\theta}{\partial R} + \frac{\partial^2 U_\theta}{\partial Z^2} + \frac{2}{R^2}\frac{\partial U_r}{\partial\theta} - \frac{U_\theta}{R^2}\right] \tag{3b}$$

Z-momentum:

$$U_r \frac{\partial U_z}{\partial R} + \frac{U_\theta}{R}\frac{\partial U_z}{\partial\theta} + U_z \frac{\partial U_z}{\partial Z}$$
$$= -\frac{1}{\rho}\frac{\partial P_{rz}}{\partial Z} + \frac{\mu}{\rho}\left[\frac{\partial^2 U_z}{\partial R^2} + \frac{1}{R}\frac{\partial U_z}{\partial R} + \frac{\partial^2 U_z}{\partial Z^2}\right] \tag{3c}$$

and the continuity equation:

$$\frac{1}{R}\frac{\partial}{\partial R}\left(RU_r\right) + \frac{1}{R}\frac{\partial}{\partial\theta}\left(U_\theta\right) + \frac{\partial}{\partial Z}\left(U_z\right) = 0 \tag{4}$$

It can be seen that there are five unknowns: the velocities components $U_r$, $U_\theta$, $U_z$, $P_\theta$ and the pressure, $P_{rz}$, in Equations (3) and (4), therefore insufficient for a solution to be determined uniquely. To close this void in the system, an additional equation is derived by considering the mass flow rate at any given cross section of the duct and its numerical value ought to be constant, or mathematically as

$$\iint_A \rho U_\theta dA = \text{constant} \tag{5}$$
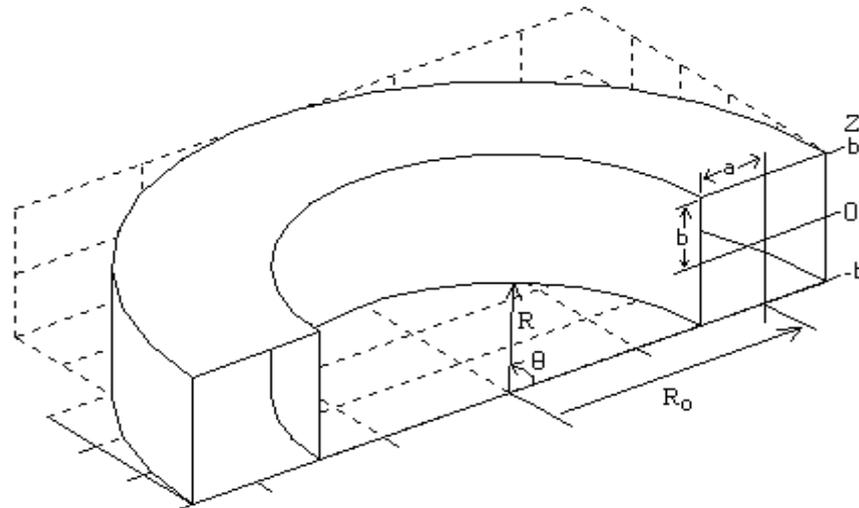
Figure 1: A curved rectangular duct and the adopted coordinate system

## 2.2    Initial and Boundary Conditions

For parabolic-flow approximation that is characterized as an initial-value problem, the velocity components and pressure at the duct inlet need to be specified. The boundary conditions at the duct outlet ($\theta=180°$) are not required due to the parabolic nature of the governing equations. It is assumed that a uniform streamwise velocity component and a uniform pressure are applied at the inlet of the duct. Besides, the transverse velocity components at the inlet are assumed to be zero. Explicitly, at the duct inlet ($\theta = 0°$):

$$U_\theta = U_o \tag{6a}$$

$$U_r = U_z = 0 \tag{6b}$$

$$P_\theta = P_{in} \tag{6c}$$

$$P_{rz} = 0 \tag{6d}$$

Alternatively, fully developed velocity profiles and pressure can be applied at the duct inlet, utterly depending on the desired type of inlet boundary conditions. At the duct wall ($R=\pm a$ or $Z=\pm b$) for all $\theta$, no slip condition is applied,

$$U_r = U_\theta = U_z = 0 \tag{6e}$$

## 3.0    SOLUTION PROCEDURE

### 3.1    Discretization

The domain of interest is discretized by grid points of spacing $\Delta R$ in the R-direction, $\Delta\theta$ in the $\theta$-direction and $\Delta Z$ in the Z-direction. i, n and k are indices

associated with R, θ and Z, respectively. With the utilization of ADI method, the limit of the streamwise step size, Δθ, is increased considerably.

### 3.2 The Scheme of Briley [7]

Since these equations have be made parabolic with respect to the streamwise direction, θ-direction, a solution at a given (θ+Δθ)-station ((n+1)-station) can be advanced from the known solution at θ-station (n-station) based on an alternating-direction implicit (ADI) method as given in Ames [19] and Lam [20]. Two Poisson equations with Neumann boundary conditions are required to be solved for each station, one to ensure the computed velocity components satisfy the continuity equation while the other is the pressure-Poisson equation.

There are four major steps in the scheme of Briley [7]. Quoting from his original paper, the procedure is as follows;

(i) The streamwise velocity, $(U_\theta)_{i,j}^{n+1}$ is computed by solving the streamwise momentum, Equation (3b) and the global mass flow relation, Equation (5), with $(P_\theta)^{n+1}$ determined implicitly through standard secant iteration technique.

(ii) Solve the transverse momentum equations, Equations (3a) and (3c), yielding approximated values of $(U_r)_{i,j}^{n+1}$ and $(U_z)_{i,j}^{n+1}$, these approximated values of the transverse velocity components are denoted by $(U_{rp})_{i,j}$ and $(U_{zp})_{i,j}$ respectively.

(iii) Small corrections for the transverse velocity components, $(U_{rc})_{i,j}$ and $(U_{zc})_{i,j}$ are computed from the requirement that the resulted transverse velocity components satisfy the continuity equation, Equation (4). Thus, the transverse velocity components are given by

$$(U_r)_{i,j}^{n+1} = (U_{rp})_{i,j} + (U_{rc})_{i,j} \qquad (7a)$$

$$(U_z)_{i,j}^{n+1} = (U_{zp})_{i,j} + (U_{zc})_{i,j} \qquad (7b)$$

(iv) $(P_{rz})_{i,j}^{n+1}$ is calculated by solving a Poisson equation that is derived from the transverse momentum Equations (3a) and (3c), which are evaluated using the corrected values of $(U_r)_{i,j}^{n+1}$ and $(U_z)_{i,j}^{n+1}$.

These four steps are then repeated for the following stations.

### 3.3 Details of Solution Procedure

In step (iii), the velocity corrections, $(U_{rc})_{i,j}$ and $(U_{zc})_{i,j}$ are determined by introducing a velocity potential such that:

$$RU_{rc} = \frac{\partial \phi}{\partial R} \qquad (8a)$$

$$RU_{zc} = \frac{\partial \phi}{\partial Z} \tag{8b}$$

A Poisson equation can be formed by substituting Equation (7) and (8) into Equation (4).

$$\frac{\partial^2 \phi}{\partial R^2} + \frac{\partial^2 \phi}{\partial Z^2} = S_C \tag{9}$$

Since a velocity potential, $\phi$, is introduced, the boundary conditions for Equation (4) change from the Dirichlet type to the Neumann type. Bearing in mind that the velocity corrections are zero at the wall, the normal derivatives of $\phi$ at the wall would also be zero, or mathematically:

$$\frac{\partial \phi}{\partial Z} = 0 \quad , \quad (R = -a, a) \tag{10a}$$

$$\frac{\partial \phi}{\partial R} = 0 \quad , \quad (Z = -b, b) \tag{10b}$$

The solution of Neumann-Poisson problem requires extra attention for Equation (9) only has a solution to an additive constant if a compatibility condition, Equation (11), relating the source term, $S_c$, and the derivative boundary condition is satisfied as in Berg and Mcgregor [21]:

$$\iint_A S_C dA = \int_C \left\{ \frac{\partial \phi}{\partial n} \right\} ds \tag{11}$$

For the present problem, this compatibility condition is not satisfied automatically. To rectify this, the error distribution method of Briley [7] which forces the source term of (9), $S_C$, to satisfy the integral constraint, Equation (11) will be adopted in the present study. The quantity E is defined by:

$$E = \frac{1}{A} \int_C \left\{ \frac{\partial \phi}{\partial n} \right\} ds - \frac{1}{A} \iint_A S_C dA \tag{12}$$

is added to the source term, $S_C$. This new source term will be called modified source term and is designated as $S_{CM}$:

$$S_{CM} = S_C + \frac{1}{A} \int_C \left\{ \frac{\partial \phi}{\partial n} \right\} ds - \frac{1}{A} \iint_A S_C dA \tag{13}$$

Having modified the source term in Equation (9), it is more appropriate to write

$$\frac{\partial^2 \phi}{\partial R^2} + \frac{\partial^2 \phi}{\partial Z^2} = S_{CM} \tag{14}$$

Meanwhile, in step (iv), the pressure-Poisson equation is formed by differentiate Equation (3a) with respect to R and Equation (3c) with respect to Z, and adding the resulted equations together:

$$\frac{\partial^2 \left(P_{rz}\right)^{n+1}}{\partial R^2} + \frac{\partial^2 \left(P_{rz}\right)^{n+1}}{\partial Z^2} = S_P \tag{15}$$

Similar to that of Equation (9) and Equation (10) is subjected to Neumann boundary conditions. Thus, modification on the source term, $S_p$, is made.

### 3.4    Modifications on the Scheme of Briley

Instead of standard secant method, $(P_0)^{n+1}$ determined implicitly through Bisection Method as in Mathews [22]. It is the experience of the present authors that those more effective schemes such as secant iterative method would occasionally fail to converge to the desired accuracy with the magnitude of the error oscillating between some values.

With the modification on the source term $S_C$, the original continuity (Equation 4) would possess a small mass source of S:

$$\frac{1}{R}\frac{\partial}{\partial R}\left(RU_r\right) + \frac{1}{R}\frac{\partial}{\partial \theta}\left(U_\theta\right) + \frac{\partial}{\partial Z}\left(U_z\right) = S \tag{16}$$

The average value of S at a given $\theta$, designated as $S_{ave}$, serves as a convenient parameter to compare the accuracy of different solutions.

In order to increase numerical stability and attain higher accuracy, it is of great essence to minimize the magnitude of S. This is done through multiple corrections to the velocity field instead of just one correction as in Briley's [7] work. After obtaining the velocity correction, $U_{rc}$ and $U_{zc}$, they are added to the predicted velocity, $U_{rp}$ and $U_{zp}$, as the newly predicted velocity to be corrected, mathematically as:

$$\left(U_{rp}\right)_{new} = U_{rp} + U_{rc} \tag{17a}$$

$$\left(U_{zp}\right)_{new} = U_{zp} + U_{zc} \tag{17b}$$

Corrections are done until the difference in the value of S for two successive corrections is less than a predefined value. It is possible to reduce the computational effort and time if in solving for $U_{rc}$ and $U_{zc}$ via Neumann-Poisson Equation (14), only a few iterations are performed. It is this modification that greatly increases the stability of the scheme, enabling computations be made for strongly curved ducts and curved converging ducts.

## 4.0   RESULTS AND DISCUSSIONS

In this section, comparisons are made with the available computations and experimental data, in order to verify the present scheme. Computations have been made on ducts of $0.01 \leq H_D/R_o \leq 0.50$ and $0.67 \leq \gamma \leq 1.5$ for De covering the range of $10 \leq De \leq 1768$, far higher that those computed by Ghia and Sokhey [6] whom used the original scheme of Briley [7]. For these computations, the average error ($S_{ave}$) is well contained in the magnitude of $10^{-4}$. To the best of our knowledge, computational and experimental data for developing flow in strongly curved ducts is only available for De up to 520, rendering comparison impossible for higher De flow. Therefore, the present study will make use of the available data of the case of $De = 520$ for a duct of $H_D/R_o = 0.4348$ rigorously. However, for ducts of smaller curvature ratio, De up to 764 has been computed, attributed to Arnal *et al.* [5], for a duct of $H_D/R_o = 0.2981$. Comparison with their results would serve as an extra mean to validate the present scheme.

To facilitate the interpretation of the numerical results, graphs are plotted with the following normalization:

$$r* = \frac{R}{a} \tag{18a}$$

$$z* = \frac{Z}{b} \tag{18b}$$

A typical case of De=54 along a duct of $H_D/R_o$=0.0690 and $\gamma$=1 under uniform entry conditions, on a (21x64x21) mesh will be considered first. The development of the streamwise velocity ($U_\theta/U_o$) along z*=0 and r*=0 is given in Figure 2a and Figure 2b respectively with the computations of Ghia and Sokhey [6] and Govindan and Lakshminarayana [8] superimposed. It is clear that the induced centrifugal force distorts the symmetrical flow along the line z*=0, shifting the region of maximum velocity towards the outer wall of the duct. On the other hand, the velocity profile remains reasonably symmetrical as it should because heat transfer and gravitational force are not considered. From these figures, it can be observed that the present computation is in fact in good agreement with that of Ghia and Sokhey [6] and Govindan and Lakshminarayana [8]. The present computation suggested that fully developed flow is achieve around θ=100° well in agreement with that of θ=103° predicted by Ghia and Sokhey [6]. Figure 2c shows the secondary velocity profiles for fully developed flow together with the results of Ghia and Sokhey [6] and Govindan and Lakshminarayana [8], and it is obvious that both qualitative and quantitative agreement is attained.
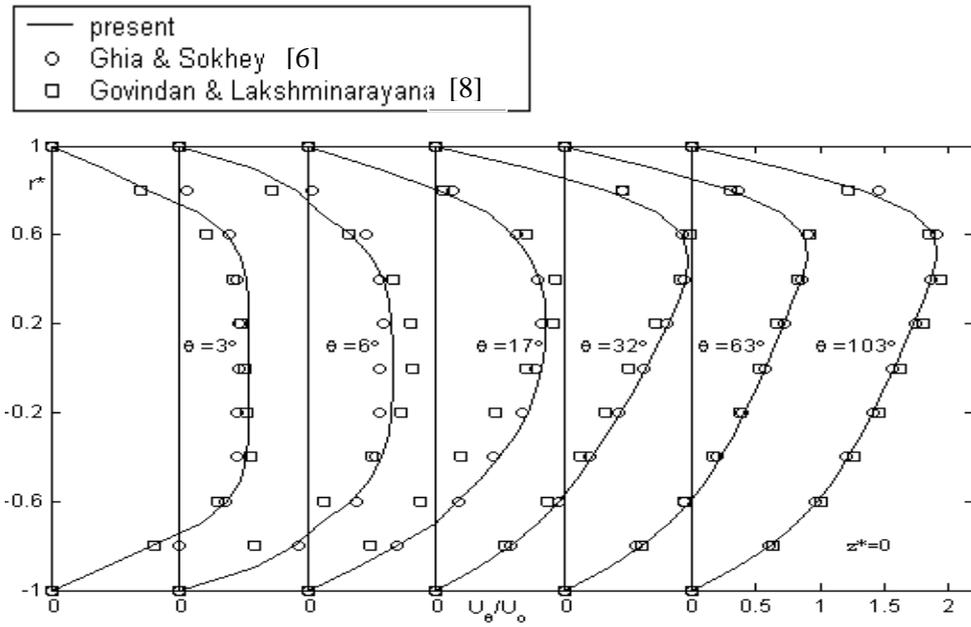
Figure 2a: Development of the streamwise velocity profile for De=54
and Re=206 along a duct of $H_D/R_o$=0.0690 and $\gamma$=1 along z*=0
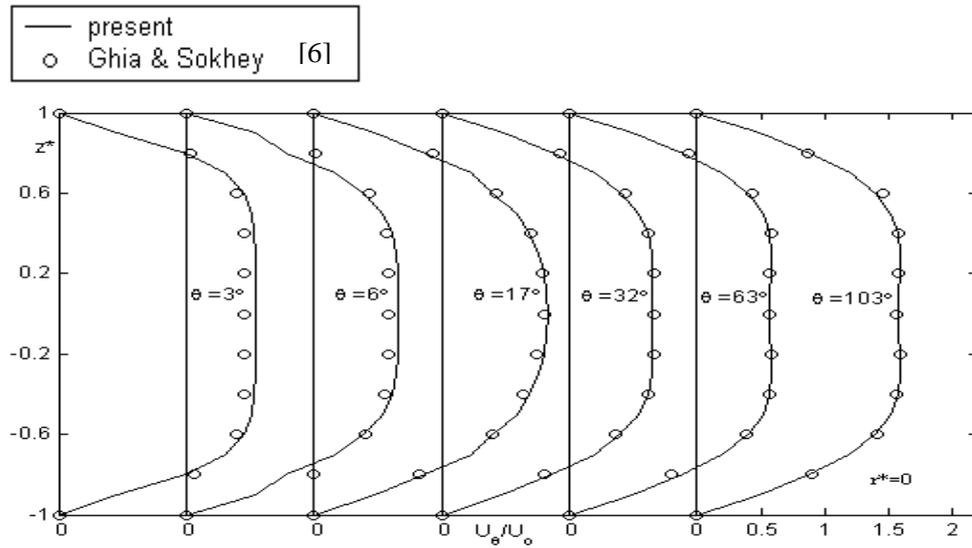


Figure 2b: Development of the streamwise velocity profile for De=54 and
Re=206 along a duct of $H_D/R_o$=0.0690 and $\gamma$=1 along r*=0

9
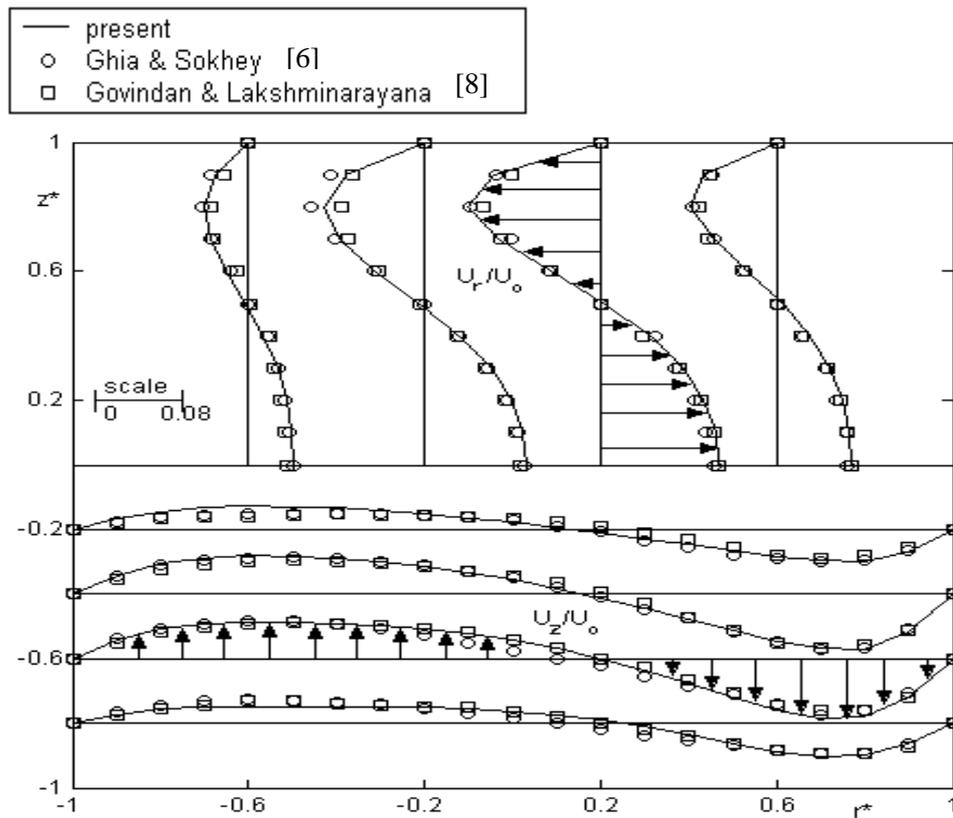
Figure 2c: Fully developed secondary velocity profiles for De=54 and
Re=206 along a duct of $H_D/R_o$=0.0690 and $\gamma$=1

For higher De but smaller $H_D/R_o$, another case in which Dean instability is found to occur, according to Ghia and Sokhey's [6] computation, was computed. For this particular case, De=142 along a duct of $H_D/R_o$=0.0274 and $\gamma$=1 subjected to uniform entry conditions on a mesh of (21 x 64 x 21) grid points. The second vortex pair starts to make its appearance at $\theta$=46° at the region near the outer wall of the duct as shown in Figure 3a. This additional vortex pair is seen to be gaining strength, pushing the fluid particles near from outer wall towards the inner wall. This would in turn shift the region of maximum streamwise velocity towards the inner wall as depicted in Figure 3b. Such action of the second vortex pair would render the formation of two region of maximum streamwise velocity (the one in the lower portion of the duct is shown in Figure 3c). From Figure 3c, it is noticed the strength of the second vortex pair can grow to a magnitude comparable to the primary vortex pair, influencing the flow field significantly. The secondary velocity profiles for fully developed flow are compared with that of Ghia and Sokhey [6] in Figure 3d where good agreement is attained.
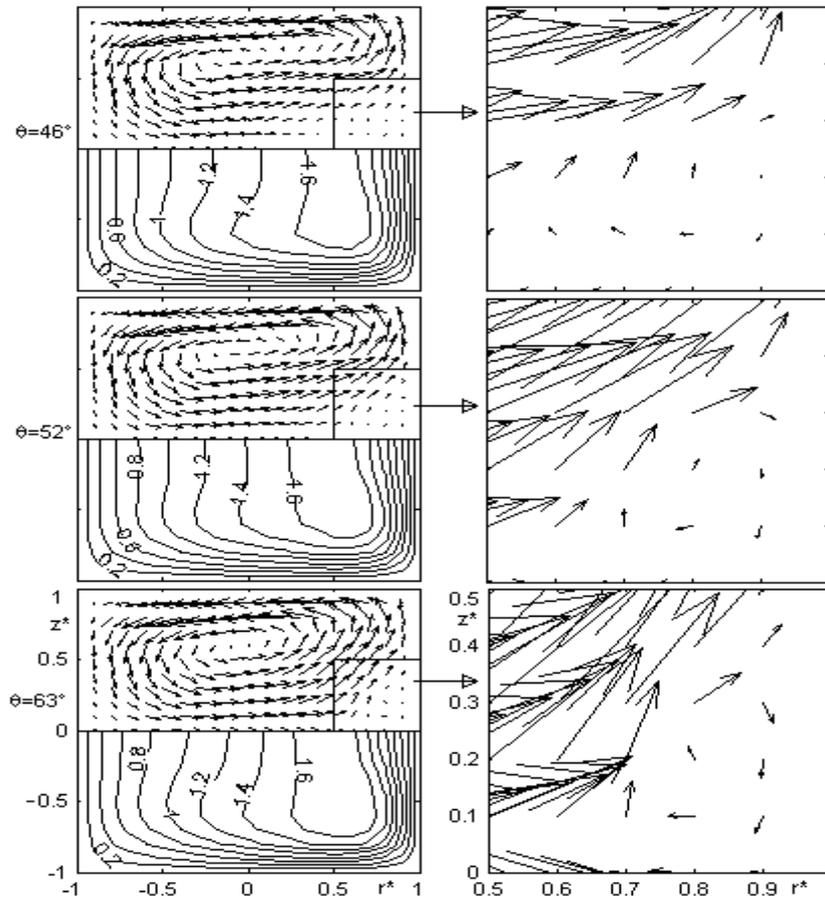
Figure 3a: Contour plots of $U_\theta/U_o$ and secondary velocity vectors plots for De=142 along a duct of $H_D/R_o$=0.0274 and $\gamma$=1 at $\theta$=46°, $\theta$=52° and $\theta$=63°
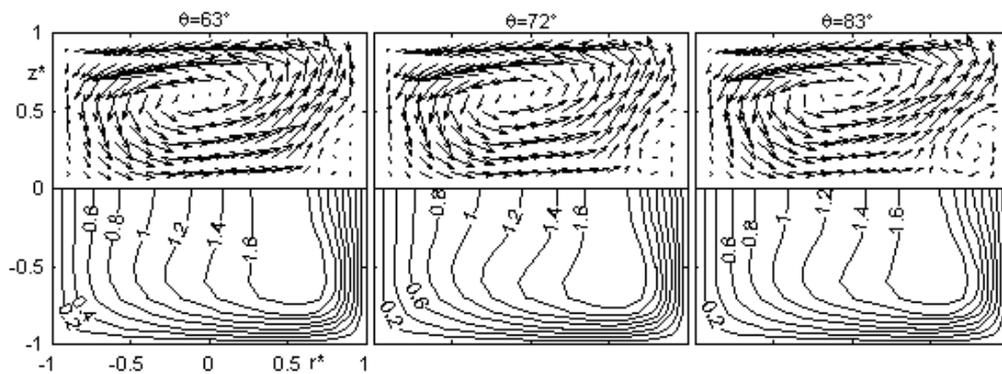


Figure 3b: Contour plots of $U_\theta/U_o$ and secondary velocity vectors plots for De=142 along a duct of $H_D/R_o$=0.0274 and $\gamma$=1 at $\theta$=63°, $\theta$=72° and $\theta$=83°
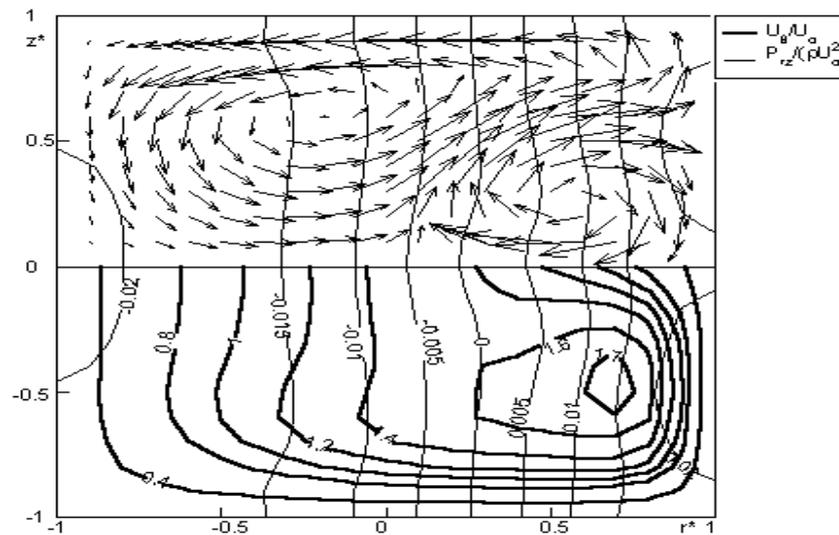
Figure 3c: Contour plot of $P_{rz}/(\rho U_o^2)$ and $U_\theta/U_o$ and secondary velocity vectors plot for De=142 along a duct of $H_D/R_o$=0.0274 and $\gamma$=1 for fully developed flow
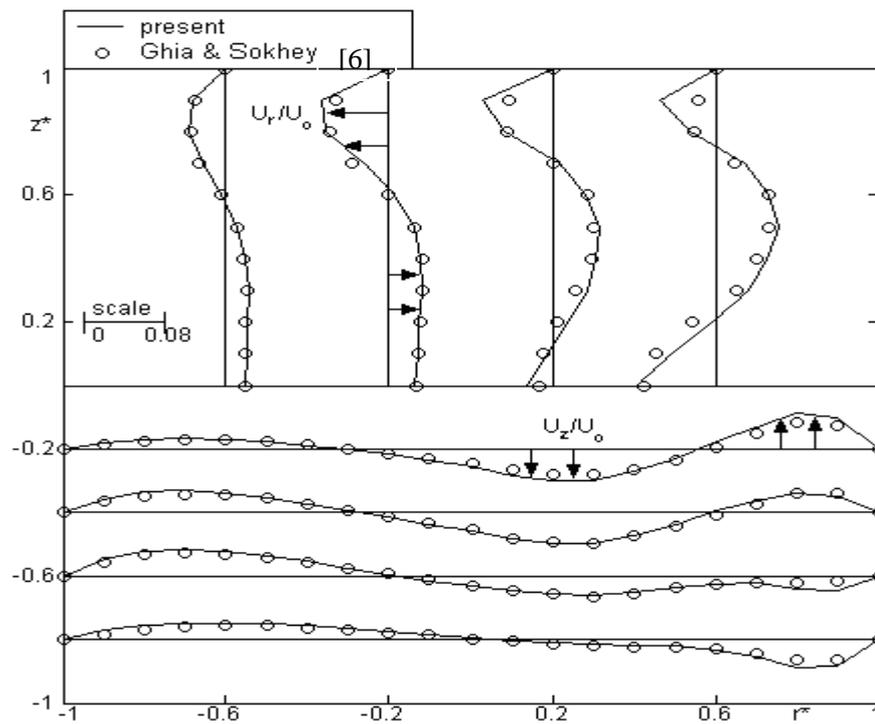


Figure 3d: Fully developed secondary velocity profiles for De=142 along a duct of $H_D/R_o$=0.0274 and $\gamma$=1

For those cases discussed, $H_D/R_o$ and De remain small. For higher $H_D/R_o$ and De, Humphrey *et al.* [9] studied, both experimentally and numerically (using PPNS equations), the developing flow through a highly curved 90° bend of $H_D/R_o$=0.4348 and $\gamma$=1 for De=520 with a fully developed flow profile (for straight duct) at the duct inlet. Later, Taylor *et al.* [12] measured the flow parameters for the same case. According to Humphrey *et al.* [9] and Taylor *et al.* [12], for large value of $H_D/R_o$, the use of PNS equations to approximate the flow becomes inadequate since the transverse pressure, $P_{rz}$, is no longer a mild function of the streamwise coordinate, $\theta$, for such a geometry. Both advocate the use of PPNS equations instead of PNS equations. However, it will be demonstrated here that the use of PNS equations could produce equally accurate results.

The streamwise velocity contour at the duct inlet for both the present computation and Humphrey *et al.* is shown in Figure 4a, which are almost the same. The present computation is done on a mesh of (41x32x41) grid points. To obtain the boundary condition at the duct inlet, the PNS equations for the viscous incompressible flow along a straight duct are solved for the fully developed flow.

With reference to Figure 4b and Figure 4c, the present computation predicts the maximum $U_\theta/U_o$ would drop to around 1.9 for $\theta$=30° and 1.7 for $\theta$=60°, far higher than the prediction of 1.7 and 1.5 by Humphrey *et al.*'s computations. However, the measurements of Humphrey *et al.* [9] do not indicate such drastic drop of streamwise velocity. The maximum $U_\theta/U_o$ only drops to around 1.7 at $\theta$=60° (Figure 4d), similar in magnitude with the present prediction. At $\theta$=60°, where both experimental and numerical data of Humphrey *et al.* are available (Figure 4c and Figure 4d), observation shows that the structure of the streamwise velocity contour of the present computation is in a better agreement, both qualitatively and quantitatively, with the measurements of Humphrey *et al.*

The contour plots of $U_\theta/U_o$ at $\theta$=90° are shown in Figure 4e and Figure 4f. At first glance, these figures reveal good agreement between the present computation with the computation and measurement of Humphrey *et al.* [9] for the outer half of the duct (0≤r*≤1, -1≤z*≤1). The computation and measurement of Humphrey *et al.* suggest the maximum value of $U_\theta/U_o$ reduces to 1.6 and 1.7 respectively, comparable to the magnitude of 1.6 to 1.7 of the present computation. On the otherhand, for the inner half of the duct (0≤r*≤1, -1≤z*≤1), Humphrey *et al.'s* computation suggests a far simpler $U_\theta/U_o$ contour than their very measurements. The perplexing structure of the $U_\theta/U_o$ contour for this portion of the duct, revealed by Humphrey *et al.'s* measurements, is captured by the present computation. It will be shown later that with such intricate feature of the $U_\theta/U_o$ contour in the flow, the secondary flow would be rather complex, consisting of several vortex pairs.

As expected, the structure of the secondary flow for such high De along a highly curved duct is very complex, consisting of more than two vortex pairs. In the present computation, four vortex pairs as depicted by the secondary velocity vectors plot in Figure 4j are captured. In the work of Rosenfeld *et al.* [14], Zang *et al.* [16] and Tamamidis *et al.* [17], three vortex pairs are observed at $\theta$=90°, instead of four pairs. These three major vortex pairs are well predicted both in terms of location and strength in the present study. However, if the secondary

velocity vectors plots of Rosenfeld *et al.* [14] and Zang *et al.* [16] are scrutinized, it seems that there is one additional small vortex pair at the region near r*=-1, z*=0. The present authors are convinced that if their computations were conducted on a finer mesh, they were able to capture this small vortex pair properly.
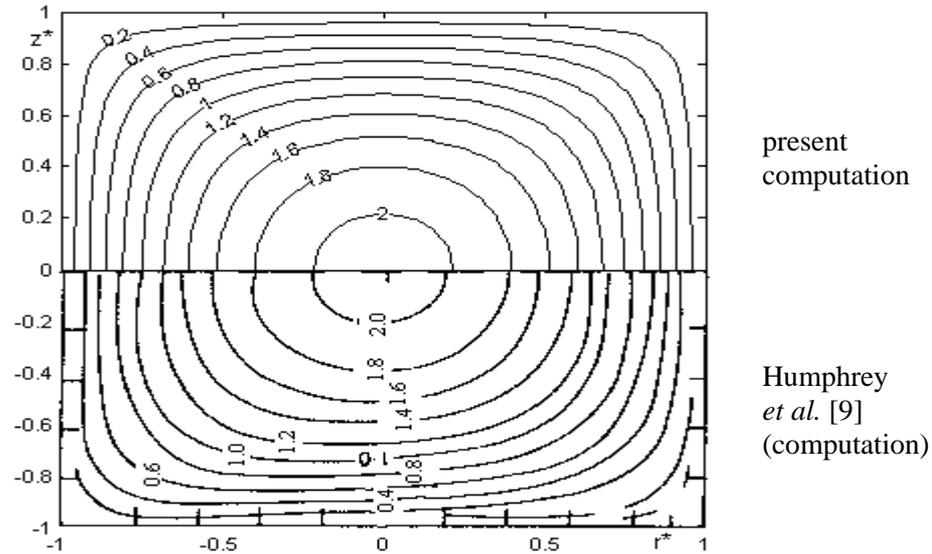


Figure 4a: Contour plots of $U_\theta/U_o$ for De=520 along a duct of $H_D/R_o=0.4348$ and $\gamma=1$ at $\theta=0°$ together with Humphrey *et al.* [9] computation
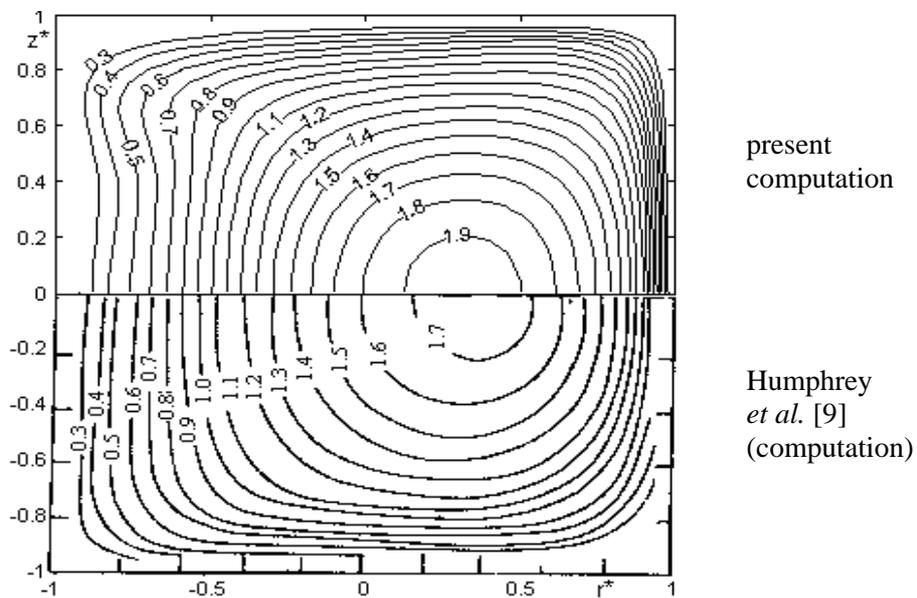


Figure 4b: Contour plots of $U_\theta/U_o$ for De=520 along a duct of $H_D/R_o=0.4348$ and $\gamma=1$ at $\theta=30°$ together with Humphrey *et al.* [9] computation

present
computation

Humphrey
*et al.* [9]
(computation)
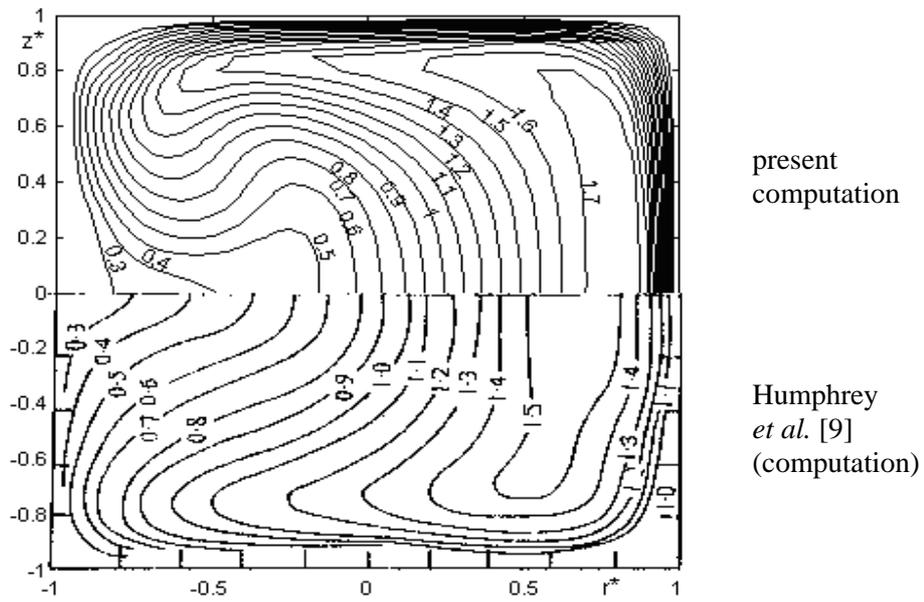
Figure 4c: Contour plots of $U_\theta/U_o$ for De=520 along a duct of $H_D/R_o$=0.4348
and $\gamma$=1 at $\theta$=60° together with Humphrey *et al.* [9] computation



Humphrey
*et al.* [9]
(measurements)

present
computation
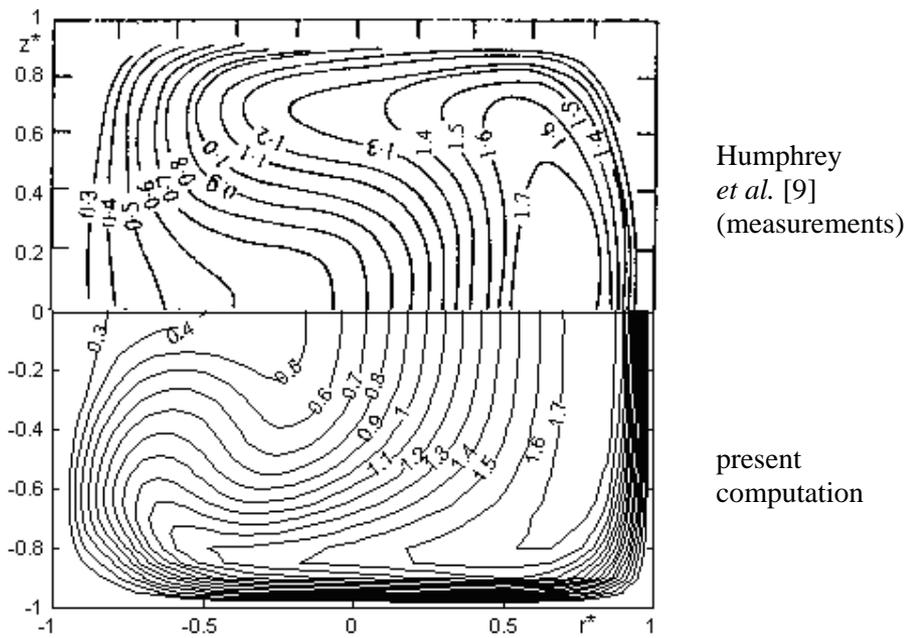
Figure 4d: Contour plots of $U_\theta/U_o$ for De=520 along a duct of $H_D/R_o$=0.4348
and $\gamma$=1 at $\theta$=60° together with Humphrey *et al.* [9] measurements
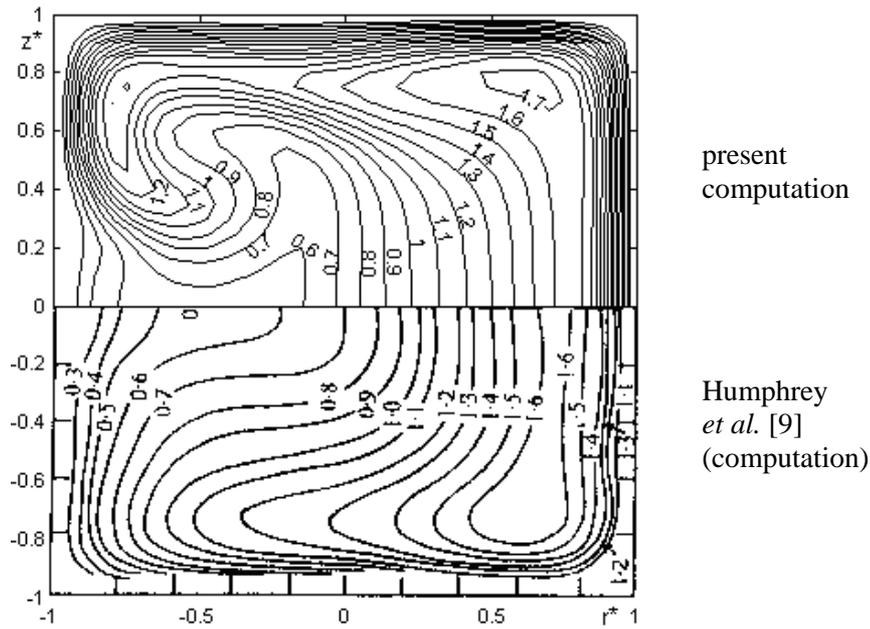
Figure 4e: Contour plots of $U_\theta/U_o$ for De=520 along a duct of $H_D/R_o$=0.4348 and $\gamma$=1 at $\theta$=90° together with Humphrey *et al.* [9] computation
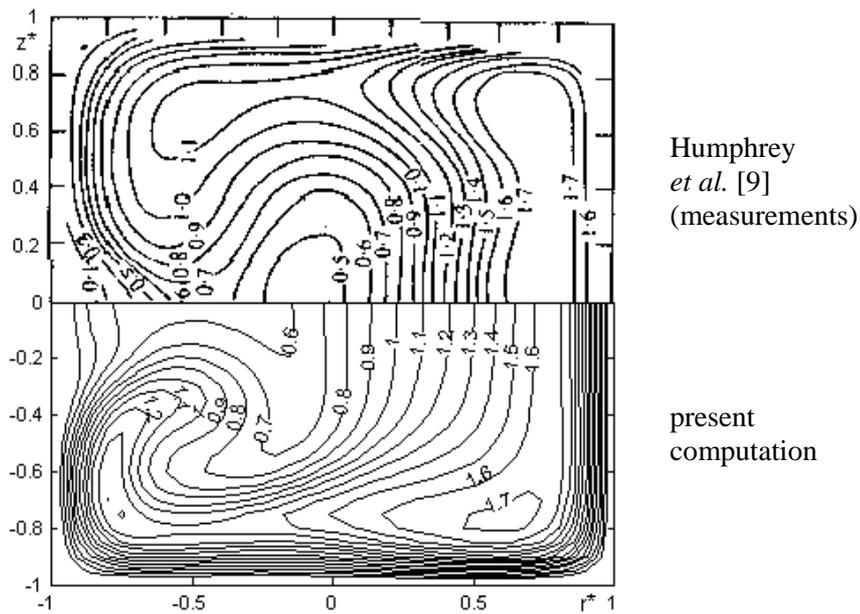


Figure 4f: Contour plots of $U_\theta/U_o$ for De=520 along a duct of $H_D/R_o$=0.434 and $\gamma$=1 at $\theta$=90° together with Humphrey *et al.* [9] measurements

present

Rosenfeld *et al.* [14]

Zang [16]

Tamamidis *et al.* [17]
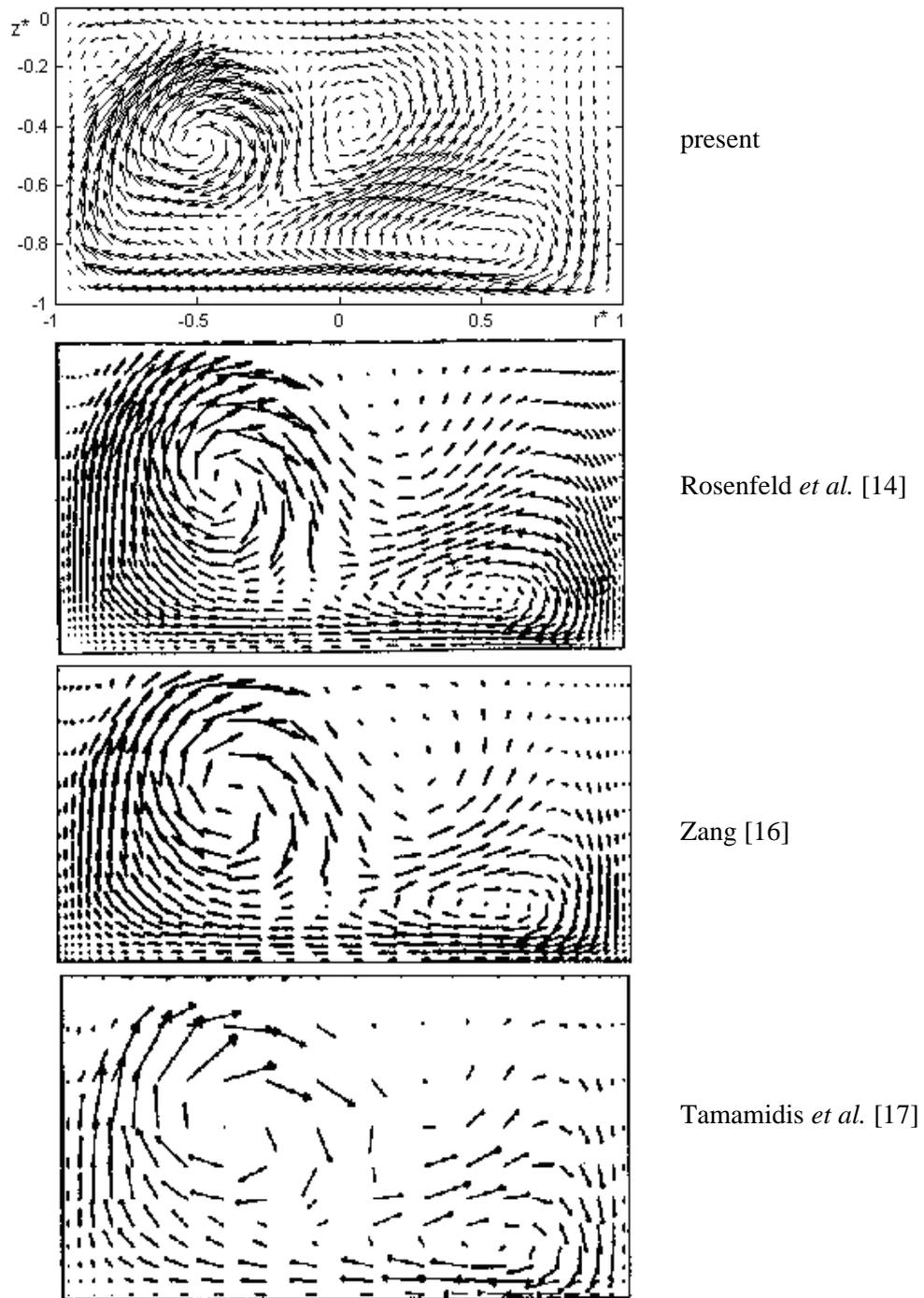
Figure 4g: Secondary velocity vectors plot for De=520 along a duct
of $H_D/R_o$=0.4348 and $\gamma$=1 at $\theta$=90°

In another study, Arnal *et al.* [15] computed the solution for De=764 along a curved duct of $H_D/R_o$= 0.2981. Figure 5a shows the streamwise velocity contour and the secondary velocity vectors plots for their computation at θ=45°. From this figure, it can be seen that the streamwise velocity predicted in the present computation is in a remarkable agreement with that of Arnal *et al.* both in terms of magnitude and the contour structure. The only discrepancy is that Arnal *et al.* predicts the maximum value of $U_\theta/U_o$ to be around 1.7 whereas for the present study, it is around 1.8. The structure of the secondary flows predicted in the present study and that of Arnal *et al.* are identical, i.e. consist of one vortex pair. However, at θ=135° (Figure 5b), the agreement between the present study with that of Arnal *et al.* is not as good as at θ=45°. There is a significant difference in the structure of the computed secondary flow. Nevertheless, the structure of the $U_\theta/U_o$ contours predicted in each study are almost the same. It is most unfortunate that experimental data of Arnal *et al.* at θ=135° is not present in their papers, thus, a more conclusive statement cannot be made regarding accuracy of both computations and the encountered discrepancy.
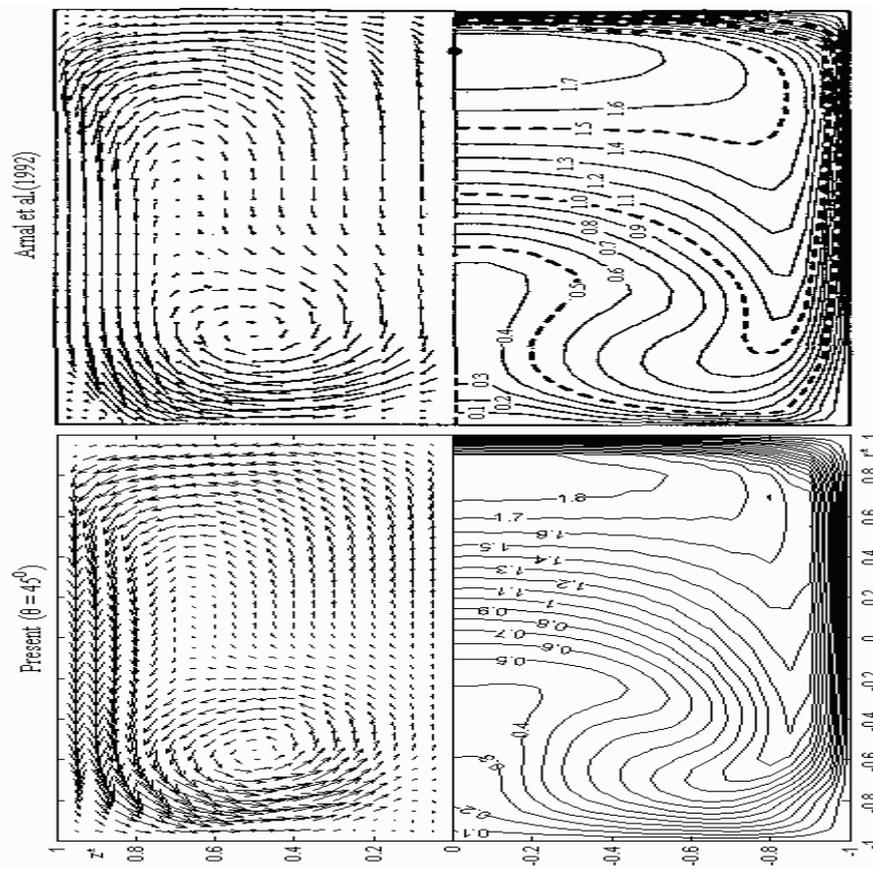


Figure 5a: Contour plots of $U_\theta/U_o$ and secondary velocity vectors plots for De=764 along a duct of $H_D/R_o$=0.2981 at θ=45°
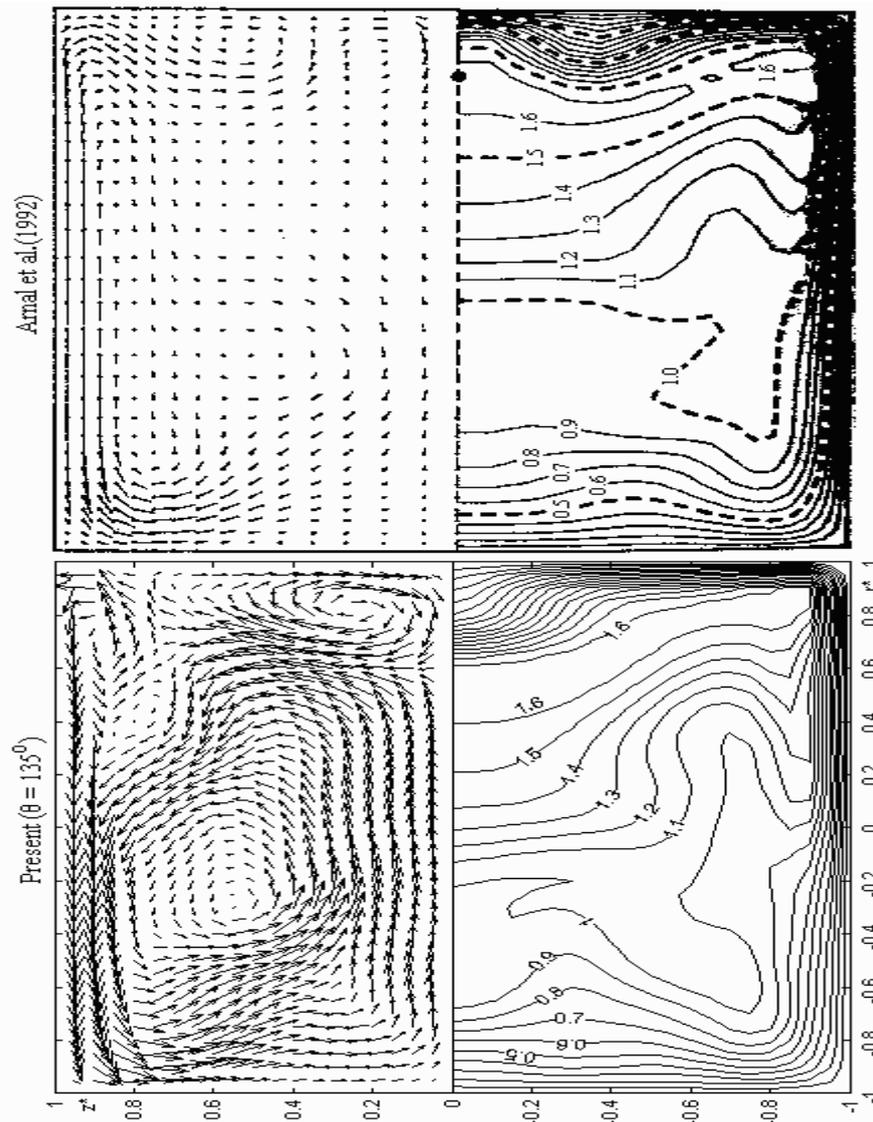
Figure 5b: Contour plots of $U_\theta/U_o$ and secondary velocity vectors plots
for De=764 along a duct of $H_D/R_o$=0.2981 at $\theta$=135°

Based on the validation done, especially the last case considered, it is deducible that PNS equations are sufficient for approximating flow in highly curved ducts for high De, given their capability to capture the complex secondary flow. Besides those discussed cases intended for the validation of the present study, computations were also made for flow of higher De. A typical case of De = 1768 along a duct of $H_D/R_o$= 0.5 and $\gamma$=1 on a mesh of [41x65x41] grid points under the influence of uniform streamwise velocity and pressure at the inlet was computed. Figure 6 shows the contour plots of $U_\theta/U_o$ and secondary velocity vectors plots for six succesive $\theta$s. The region of maximum $U_\theta/U_o$ is in fact very low, around 1.3 at $\theta$=180°, which is an indication of developing flow. Obviously, the flow would

required a much larger θ to achieve fully developed flow and possibly would never attain it physically unless finite pitch is introduced to the duct. The secondary flow structure is excessively intrisic, consisting of more than two vortex pairs. The center of the primary vortex is located very near the inner wall as at θ=60° and θ=90° in Figure 6. Several secondary vortex pairs start making their appearance for θ>90°, distorting the structure of the primary vortex pair considerably.

## 5.0   CONCLUSION

The numerical results should the parabolised Navier-Stokes is able to appreciate secondary flow in curved rectangular regular ducts. The numerical results show good agreements with the experimental results performed by researchers in the field of secondary flow. The numerical stability as experienced by Briley, W.R. [7] is fully eliminated in the present study.
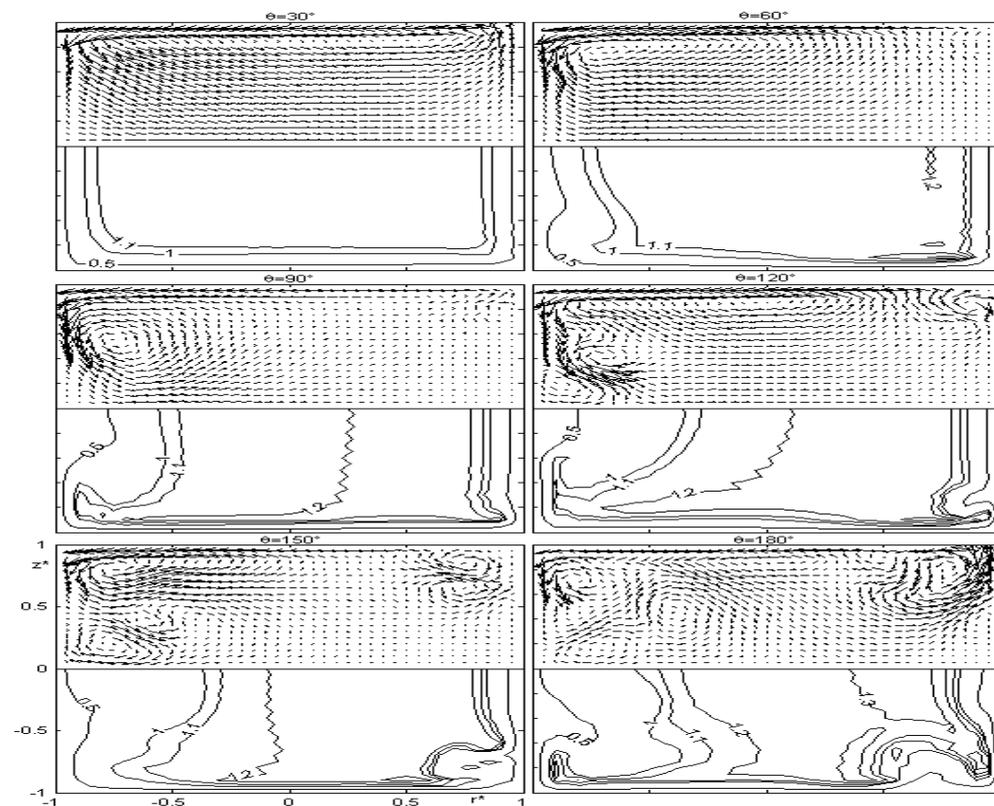


Figure 6:  Contour plots of $U_\theta/U_o$ and secondary velocity vectors plots for
De=1768 along a duct of $H_D/R_o$=0.5 and γ=1 at θ=30°,
θ=60°,θ=90°, θ=120°, θ=150° and θ=180°

## REFERENCES

1. Patankar, S.V., Pratap, V.S. and Spalding, D.B., 1974. Prediction of Laminar Flow and Heat Transfer in Hellically Coiled Pipes, *Journal of Fluid Mechanics*, Vol. 62, Part 3, 539-551.
2. Patankar, S.V. and Spalding, D.B., 1972. A Calculation Procedure for Heat and Mass and Momentum Transfer in Three Dimensional Parabolic Flows, *International Journal of Heat and Mass Transfer*, Vol. 15, 1787-1806.
3. Mori, Y. and Nakayama, W., 1965. Study of Forced Convective Heat Tansfer in Curved Pipes (1st report, Laminar Region), *International Journal of Heat and Mass Transfer*, Vol. 8, 67.
4. Austin, L.R., 1971. The Development of Viscous Flow Within Helical Coils, *Ph.D. Thesis*, University of Utah.
5. Akiyama, M. and Cheng, K.C., 1971. Boundary Vorticity Method for Laminar Force Convection Heat Transfer in Curved Circular Pipes, *International Journal of Heat and Mass Transfer*, Vol. 14, 1659.
6. Ghia, K.N. and Sokhey, J.S., 1977. Laminar Incompressible Viscous Flow in Curved Ducts of Regular Cross Sections, *Transactions of the ASME Journal of Fluids Engineering*, 640-648.
7. Briley, W.R., 1974. Numerical Method for Predicting Three-Dimensional Steady Viscous Flow in Ducts, *Journal of Computational Physics*, Vol. 14, 8-28.
8. Govindan, T.R. and Lakshminarayana, B., 1988. A Space-Marching Method for the Computation of Viscous Internal Flows, *Computers and Fluids*, Vol. 16, No. 1, 21-39.
9. Humphrey, A.C., Taylor, A.M.K. and Whitelaw, J.H., 1977. Laminar Flow in A Square Duct of Strong Curvature, *Journal of Fluid Mechanics*, Vol. 83, Part 3, 509-527.
10. Pratap, V.S. and Spalding, D.B., 1976. Fluid Flow and Heat Transfer in Three-dimensional Duct Flows, *International Journal of Heat and Mass Transfer*, Vol. 19, 1183-1188.
11. Pouagare, M. and Lakshminarayana, B., 1986. A Space-Marching Method for Viscous Incompressible Internal Flows, *Journal of Computational Physics*, Vol. 64, 389-415.
12. Taylor, A.M.K.P., Whitelaw, J.H. and Yianneskis, M., 1981. Measurements of Laminar and Turbulent Flow in a Curved Duct with Thin Inlet Boundary Layers, NASA CR-3367.
13. Yap, Y.F., 2002. Numerical Study of the Flow along A Curved Converging Rectangular Duct, *Master thesis*, Universiti Teknologi Malaysia.
14. Rosenfeld, M., Kwak, D. and Vinokur, M., 1991. A Fractional Step Solution Method for the Unsteady Incompressible Navier-Stokes Equations in Generalized Coordinate Systems, *Journal of Computational Physics*, Vol. 94, 102-137.
15. Arnal, M.P., Goering, D.J. and Humphrey, J.A.C., 1992. Unsteady Laminar Flow Developing in a Curved Duct, *International Journal of Heat and Fluid Flow*, Vol. 13, No. 4, 347-357.

16. Zang, Y., Street, L.B. and Koseff, J., 1994. A Non-staggered Grid, Fractional Step Method for Time-Dependent Incompressible Navier-Stokes Equations in Curvilinear Coodinates, *Journal of Computational Physics*, Vol. 114, 18-33.

17. Tamamidis, P., Zhang, G. and Assanis, D.N., 1996. Comparison of Pressure-Based and Artificial Compressibility for Solving 3D Steady Incompressible Viscous Flows, *Journal of Computational Physics*, Vol. 124, 1-13.

18. Tannehill, J.C., Anderson, D.A. and Pletcher, R.H., 1997. *Computational Fluid Mechanics and Heat Transfer,* Washington: Taylor and Francis.

19. Ames, F.W., 1992. *Numerical Methods for Partial Differential Equations*, London: Academic Press, Inc.

20. Lam, C.Y., 1994. *Applied Numerical Methods for Partial Differential Equations: An Introduction with Spreadsheet Programs*, Singapore: Simon & Schuster (Asia) Pte. Ltd.

21. Berg, P.W and Mcgregor, J.L., 1969. *Elementary Partial Differential Equations*, California: Holden-Day.

22. Mathews, J.H., 1992. *Numerical Methods for Mathematics, Science and Engineering*, 2nd edition, New Jersey: Prentice-Hall, Inc.